

# Discharge coefficient analysis for triangular sharp-crested weirs using a low-speed photographic technique

by

Bautista-Capetillo C.<sup>1\*</sup> M. ASCE, Robles O.<sup>2</sup>, Júnez-Ferreira H.<sup>3</sup>, Playán E.<sup>4</sup>

## **Abstract**

Triangular weirs are commonly used for the measurement of discharge in open channel flow, representing an inexpensive, reliable methodology for the monitoring of water allocation. In this work, a low-speed photographic technique was used to characterize the upper and lower nappe profiles of flow over fully aerated triangular weirs. A total of 112 experiments were performed covering a range of weir vertex angles (from 30° to 90°), crest elevations (8 or 10 cm) and discharges (0.01 - 7.82 l s<sup>-1</sup>). The experimental nappe profiles were mathematically modeled and combined with elements of free-vortex theory to derive a predictive equation for the weir discharge coefficient. Comparisons were established between measured  $C_d$ , the proposed discharge coefficient equation and discharge coefficient equations identified in the literature. The proposed equation can predict  $C_d$  with a Mean Estimation Error (MEE) of 0.001, a Root

---

<sup>1</sup> Professor, Recursos Hidráulicos, Universidad Autónoma de Zacatecas, Av. Ramón López Velarde 801, 98000 Zacatecas, Mexico.

<sup>2</sup> Master Degree Student, Maestría en Ingeniería Aplicada Orientación en Recursos Hidráulicos, Universidad Autónoma de Zacatecas, Av. Ramón López Velarde 801, 98000 Zacatecas, Mexico.

<sup>3</sup> Professor, Recursos Hidráulicos, Universidad Autónoma de Zacatecas, Av. Ramón López Velarde 801, 98000 Zacatecas, Mexico.

<sup>4</sup> Research Professor, Departamento Suelo y Agua, Estación Experimental de Aula Dei, CSIC. P. O. Box 13034. 50080 Zaragoza, Spain.

\* Corresponding author: [baucap@uaz.edu.mx](mailto:baucap@uaz.edu.mx)

18 Mean Square Error (RMSE) of 0.004, and an Index of Agreement (IA) of 0.984. In the  
19 experimental conditions of this study, this performance slightly improves that of the  
20 equation proposed by Greve in 1932, showing the same absolute value of MEE, but  
21 lower values of RMSE and IA.

22 **Keywords:** weir vertex angle, flow measurement, hydrometry, free-vortex theory

## 23 Introduction

24 Weirs are elevated barriers located perpendicular to the main direction of water  
25 movement to cause the fluid to rise above the obstruction in order to flow through an  
26 opening of regular shape. For a properly designed and operated weir of a given  
27 geometry there is a unique discharge corresponding to each measurement of flow depth  
28 (El-Hady 2011). The geometrical parameters involved in the hydraulic operation of  
29 weirs are the length of the weir crest and the shape of the flow control section (Emiroglu  
30 et al. 2010; USBR 2001). In sharp-crested or thin-plate weirs the upstream head ( $h$ ) to  
31 length of crest in the direction of flow ( $L$ ) ratio is greater than 15 (Fig. 1). Specific  
32 assumptions are adopted to estimate the relation between discharge and upstream head  
33 (Bagheri and Heidarpour 2010; Sotelo 2009; El-Alfy 2005; Bos 1989). These structures  
34 have been extensively studied using classical physics and experimental analyses to  
35 understand the characteristics of flow as well as to determine the coefficient of discharge  
36 ( $C_d$ ). This coefficient represents the effects not taken into consideration in the derivation  
37 of the equations used to estimate discharge from flow depth. Such effects include  
38 viscosity, capillarity, surface tension, velocity distribution in the approach section and  
39 streamline curvature due to weir contraction (Aydin et al. 2011; El-Hady 2011).

40 In the particular case of triangular sharp-crested weirs, Shen (1981) described  
41 experimental procedures used by different authors to determine  $C_d$ . El-Alfy (2005)  
42 experimentally evaluated the effect of vertical flow curvature on the discharge  
43 coefficient, and reported that  $C_d$  is inversely proportional to the V-notch angle ( $\theta$ ) and  
44 directly proportional to the relative head ( $h/P$ ). Recently, Bagheri and Heidarpour

45 (2010) obtained a discharge coefficient equation for rectangular sharp-crested weirs  
46 based on the upper and lower nappe profiles and free-vortex theory.

47 Photography has been used for the characterization of flow over hydraulic structures,  
48 particularly weirs. For instance, Del Giudice et al., (1999) used photographs to illustrate  
49 complex flow patterns near a sewer sideweir. Novak et al. (2013) photographed the  
50 planes displayed by a laser on the flow near a side weir, and used these images to  
51 determine flow depth profiles and flow velocity (from the movement of hydrogen  
52 bubbles). Photography was recently applied to a different hydraulic problem: the  
53 characterization of sprinkler irrigation drops moving in the air. Salvador et al. (2009)  
54 and Bautista et al. (2009) performed out-door and in-door experiments to evaluate drop  
55 geometrical and kinematic characteristics using a low-speed photographic technique.

56 The objective of this study was to determine a discharge coefficient equation for  
57 triangular sharp-crested weirs based on: 1) the free vortex theory as described by  
58 Bagheri and Heidarpour (2010); and 2) measurements of the upper and lower nappe  
59 profiles using an adaptation of the low-speed photographic technique proposed by  
60 Salvador et al. (2009).

## 61 Materials and methods

### 62 **Governing equations**

63 For a sharp-crested weir of any geometrical section with the crest elevation ( $P$ ) being  
 64 high enough to neglect the velocity head (Figure 1), discharge equations are usually  
 65 obtained from the mathematical integration of an elemental flow strip over the nappe  
 66 (Singh et al. 2010). The total discharge flowing between elevations 0 and  $h$  can be  
 67 obtained solving the following expression:

$$Q = 2\sqrt{2g} C_d \int_0^h x(h-y)^{\frac{1}{2}} dy \quad [1]$$

68 where  $Q$  is the discharge over the weir ( $\text{m}^3 \text{s}^{-1}$ );  $g$  is the gravitational acceleration ( $\text{m s}^{-2}$ );  
 69  $C_d$  is the discharge coefficient (dimensionless);  $h$  is the water head (m);  $x$  is the flow  
 70 width, with  $x = f(y)$  depending of the weir geometry; and  $dy$  is the vertical thickness of  
 71 elemental flow strip. A sharp-crested weir with symmetrical triangular section and  
 72 vertex angle ( $\theta$ ) entails that  $x = y \tan\left(\frac{\theta}{2}\right)$ , as shown in Figure 1b. The resulting discharge  
 73 equation is:

$$Q = \frac{8}{15} C_d \sqrt{2g} \tan\left(\frac{\theta}{2}\right) h^{\frac{5}{2}} \quad [2]$$

74 Considering free-vortex motion theory, Bagheri and Heidarpour (2010) proposed an  
 75 expression to derive the discharge coefficient of flow passing over a rectangular sharp-  
 76 crested weir. Following the reasoning of these authors, a similar expression could be  
 77 obtained for a triangular sharp-crested weir (Equation 3):

$$Q = 2V_b R_b \tan\left(\frac{\theta}{2}\right) \left[ kY + R_b \ln\left(\frac{R_b}{kY + R_b}\right) \right] \quad [3]$$

78 where  $V_b$  is the lower nappe velocity, obtained at the section of maximum elevation of  
 79 the lower nappe ( $\text{m s}^{-1}$ );  $R_b$  is the radius of streamline curvature at lower nappe of the  
 80 profile in segment OB (m);  $k$  is the non-concentricity coefficient; and  $Y$  is the flow depth  
 81 at the section of maximum elevation of lower nappe (m) (Figure 1).

### 82 **Experimental setup and measuring techniques**

83 Experiments were performed in a horizontal rectangular recirculating plexiglass  
 84 laboratory channel 7.2 m long, 0.3 m wide, and 0.3 m high. Canal cross section was  
 85 designed for a maximum discharge of  $10 \text{ l s}^{-1}$ , having in mind a common application of  
 86 this type of weirs: the analysis of furrow irrigation inflow and outflow. Mild steel plates  
 87 (galvanized sheet metal) with a thickness of 1.5 mm were used to manufacture weirs.  
 88 Vertex angles were  $30^\circ$ ,  $45^\circ$ ,  $60^\circ$  and  $90^\circ$ , each of them with 8 and 10 cm of crest height.  
 89 Water was supplied to the channel through an overhead tank provided with an  
 90 overflow arrangement to maintain constant head. A grid wall was installed into the  
 91 channel to dissipate flow velocity. To avoid the area of water surface draw-down, head  
 92 over the weir was measured 1.0 m upstream of the vertical weir plane using a point  
 93 gage with accuracy of  $\pm 0.1 \text{ mm}$ . Discharge over the weirs was volumetrically measured,  
 94 using a prismatic steel measuring tank with base dimensions of  $0.75 \text{ m} \times 0.75 \text{ m}$ . Weirs  
 95 were installed at the end of the channel to provide an unrestricted supply of air under  
 96 the nappe. Consequently, all data for this study correspond to the conditions of fully  
 97 aerated flow. Equations of flow nappe profiles and discharge coefficients for triangular

98 sharp-crested weirs were obtained for four different models. Table 1 presents a  
99 summary of the weir characteristics and test conditions. Weir models were tested using  
100 14 flow rates. A total of 112 experiments were conducted (4 vertex angles x 2 values of P  
101 x 14 flow rates). Additionally, each discharge was measured five times. The average of  
102 these replications was used to obtain the discharge coefficient.

103 An adaptation of the low-speed photographic technique proposed by Salvador et al.  
104 (2009) was implemented in order to identify a set of points ( $z, y$ ) along the upper and  
105 lower nappes to characterize the profiles. Coordinate  $z$  corresponds to the horizontal  
106 distance downstream from the weir. All coordinate values were initially registered in  
107 pixels and then transformed to millimeters using the pixel per millimeter ratio obtained  
108 from image analysis (all images included a reference ruler). In order to assess the  
109 differences between measured-estimated values and different estimation equations  
110 proposed by other authors, the following statistic parameters were used: mean  
111 estimation error (MEE), root mean square error (RMSE), and index of agreement (IA)  
112 (Willmott, 1982).

## 113 Results

114 The points obtained from the photographs were plotted as shown in Figure 2, where  $y$  is  
 115 the vertical depth of flow at  $z$  distance downstream from the weir. Plotted information  
 116 corresponds to all measured upper and lower flow nappe profiles for the different  
 117 values of vertex angle. Figure 2 shows pairs  $(z, y)$  relative to head  $(h)$  as well as the  
 118 polynomials that best fit each case. The upper and lower nappe profiles could be  
 119 successfully adjusted to quadratic equations. Polynomials were used to determine  
 120 distances  $OA$ ,  $OB$ ,  $AC$ , and  $AE$  (Figure 1) for each weir model using the general  
 121 regression equations in Figure 2. The same procedure was used to determine the mean  
 122 radius of curvature of the streamline along the distance of  $OB$  at lower nappe profiles  
 123 ( $R_b$ ), the flow depth at the section of maximum elevation of the lower nappe ( $Y$ ), and the  
 124 correction coefficient of non-concentricity streamline ( $k$ ) (Bagheri and Heidarpour,  
 125 2010). The analysis of ratios  $R_b/h$  and  $Y/h$  against weir vertex angle expressed as  
 126  $\tan(\theta/2)$  shows potential relations in both cases. Regarding the non-concentricity  
 127 coefficient, the best relation between  $k$  and  $h \tan(\theta/2)$  is represented by a potential  
 128 equation. Substituting  $R_b/h$ ,  $Y/h$ , and  $k$  expressions into Equation 3 results in Equation  
 129 4:

$$Q = 8.859h^{\frac{5}{2}} \tan\left(\frac{\theta}{2}\right) Z_1 \left[ kZ_0 + Z_1 \ln\left(\frac{Z_1}{kZ_0 + Z_1}\right) \right] \quad [4]$$

130 where

$$Z_0 = 0.682 \left[ \tan\left(\frac{\theta}{2}\right) \right]^{0.044} \quad [5]$$



131 and

$$Z_1 = 0.445 \left[ \tan\left(\frac{\theta}{2}\right) \right]^{-0.098} \quad [6]$$

132 Combining Equations 2 and 4, the discharge coefficient can be expressed as Equation 7:

$$C_d = 3.750Z_1 \left[ kZ_0 + Z_1 \ln\left(\frac{Z_1}{kZ_0 + Z_1}\right) \right] \quad [7]$$

133 Estimated discharge coefficients (for head over the weir ranging from 1.5 cm to 15 cm)  
 134 ranged between 0.669-0.607, 0.674-0.614, 0.677-0.618, and 0.680-0.624 for weir angles of  
 135 30°, 45°, 60°, and 90° respectively. Measured discharge coefficients (for heads over the  
 136 weir of 1.5-15 cm for weir angles of 30°, 45°, and 60°; and for heads over the weir of 1.5-  
 137 12 cm for a weir angle of 90°) ranged between 0.665-0.614, 0.668-0.616, 0.672-0.620, and  
 138 0.677-0.624 for the same weir vertex angles. Figure 3 presents a comparison of the  
 139 experimental data, the proposed discharge coefficient (Equation 7) and the estimates  
 140 obtained using some references discussed by Shen (1981). The proposed equation can  
 141 predict  $C_d$  for the range or 30°-90° weir vertex angles with MME = 0.001, RMSE = 0.004,  
 142 and IA = 0.984. In the experimental conditions of this study, this performance can only  
 143 be compared to that of the equation proposed by Greve (1932), which showed the same  
 144 absolute value of MEE but lower values of RMSE and IA.

## 145 Conclusions

146 An experimental analysis was performed to estimate the discharge coefficient for four  
147 triangular sharp-crested weir models. Regression equations of the upper and lower  
148 nappe profiles developed from experimental data and free-vortex theory were used to  
149 derive a discharge coefficient equation as a function of head over the weir ( $h$ ) and weir  
150 vertex angle expressed as  $\tan(\theta/2)$ . Experimental data showed that both nappe profiles  
151 can be successfully represented by second-degree polynomials. Results also indicated  
152 that the non-dimensional mean radius of curvature of the streamline along the distance  
153 OB at lower nappe profiles ( $R_b/h$ ) and the non-dimensional flow depth at the section of  
154 maximum elevation of the lower nappe ( $Y/h$ ) show potential relations with the weir  
155 vertex angle expressed as  $\tan(\theta/2)$ . To take into account the non-concentricity of the  
156 streamlines, a correction coefficient was proposed as a function of  $h$  and  $\theta$ . Comparisons  
157 between measured  $C_d$ , the proposed discharge coefficient equation and discharge  
158 coefficient equations proposed by a number of authors were established. In the  
159 experimental conditions, the proposed equation represents an improvement in the  
160 estimation of discharge from triangular weirs, and confirms the validity of a predictive  
161 equation proposed by Greve in 1932.

162 **Acknowledgements**

163 This research was funded by the Secretaría de Agricultura, Ganadería, Desarrollo Rural,  
164 Pesca y Alimentación of the Mexican Government (SAGARPA, Mexico) and the  
165 Secretaría del Campo of Zacatecas State Government (SECAMPO, Zacatecas). Thanks  
166 are also due to the Universidad Autónoma of Zacatecas, Mexico. Cruz Octavio Robles  
167 Roveló received a scholarship from the Mexican Consejo Nacional de Ciencia y  
168 Tecnología (CONACYT).

169 **References**

- 170 Aydin, I., Altan-Sakarya, A. B., and Sisman, C. (2011). "Discharge formula for  
171 rectangular sharp-crested weirs." *Flow Measurement and Instrumentation*, 22: 144-151.
- 172 Bagheri, S., and Heidarpour, M. (2010). "Flow over rectangular sharp-crested weirs"  
173 *Irrigation Science*, 28:173-179.
- 174 Bautista-Capetillo, C. F., Salvador, R., Burguete, J., Montero, J., Tarjuelo, J. M., Zapata,  
175 N., González, J., and Playán, E. (2009). "Comparing methodologies for the  
176 characterization of water drops emitted by an irrigation sprinkler." *Transactions of the*  
177 *ASABE* 52(5): 1493-1504.
- 178 Bos, M. G. (1989). *Discharge measurement structures*. International Institute for Land  
179 Reclamation and Improvement, ILRI, Wageningen, Netherlands.
- 180 Del Giudice, G., and Hager, W. H. (1999). "Sewer sideweir with throttling pipe." *Journal*  
181 *of Irrigation and Drainage Engineering-ASCE* 125(5):298-306.
- 182 El-Alfy, K. M. (2005). "Effect of vertical curvature of flow at weir crest on discharge  
183 coefficient". *Ninth International Water Technology Conference, Sharm El-Sheikh, Egypt*,  
184 249-262.
- 185 El-Hady, R. M. A. (2011). "2D-3D modeling of flow over sharp-crested weirs." *Journal of*  
186 *Applied Sciences Research*, 7(12): 2495-2505.

- 187 Emiroglu, M. E., Kaya, N., and Agaccioglu, H. (2010). "Discharge capacity of labyrinth  
188 side weir located on a straight channel." *Journal of Irrigation and Drainage Engineering*  
189 *ASCE*, 136(1): 37-46.
- 190 Novak, G., Kozelj, D., Steinman, F. and Bajcar, T. (2013). "Study of flow at side weir in  
191 narrow flume using visualization techniques." *Flow Measurement and Instrumentation*  
192 29:45-51.
- 193 Salvador R., Bautista-Capetillo C., Burguete J., Zapata N., and Playán, E. (2009). "A  
194 photographic methodology for drop characterization in agricultural sprinklers."  
195 *Irrigation Science*, 27(4): 307-317.
- 196 Shen, J. (1981). *Discharge characteristics of triangular-notch thin-plate weirs*. Studies of flow  
197 of water over weirs and dams. Geological Survey Water-Supply Paper 1617-B,  
198 Washington D. C.
- 199 Singh, N. P., Yada, S. M., and Singh, R. (2010). "Behavior of sharp crested weirs of  
200 various curvilinear shapes." *Proceedings of the 13th Asian Congress of Fluid Mechanics*,  
201 17-21, Dhaka, Bangladesh.
- 202 Sotelo, G. (2009). *Hidráulica general I: Fundamentos*. Ed. LIMUSA, Mexico.
- 203 United States Bureau of Reclamation (2001). *Water measurement manual*. Revised reprint.  
204 Denver, Colorado.
- 205 Willmott C. J. (1982). "Some comments on the evaluation of model performance."  
206 *Bulletin American Meteorological Society*, 63(11): 1309-1313.

207 **List of Tables**

208 **Table 1.** *Triangular sharp-crested weir characteristics and test conditions.*

209

210 **List of Figures**

211 **Figure 1.** *Experimental parameters: a) direction of flow view, b) frontal view.*

212 **Figure 2.** *Upper and lower nappe profiles. Weir vertex angles: a) 30°, b) 45°, c) 60°, and d) 90°.*

213 **Figure 3.** *Discharge coefficient ( $C_d$ ) vs. head over triangular sharp-crested weir. Weir vertex*  
214 *angles: a) 30°, b) 45°, c) 60°, and d) 90°.*

**Table 1.** *Triangular sharp-crested weir characteristics and test conditions.*

<b>Weir model</b>	<b>Vertex angle (<math>\theta</math>, °)</b>	<b>P (cm)</b>	<b>Q (l s<sup>-1</sup>)</b>	<b>h (cm)</b>
1	30	8, 10	0.01-3.56	1.5-15.0
2	45	8, 10	0.02-5.52	1.5-15.0
3	60	8, 10	0.03-7.74	1.5-15.0
4	90	8, 10	0.04-7.82	1.5-12.0

**Figure 1.** *Experimental parameters: a) direction of flow view, b) frontal view.*

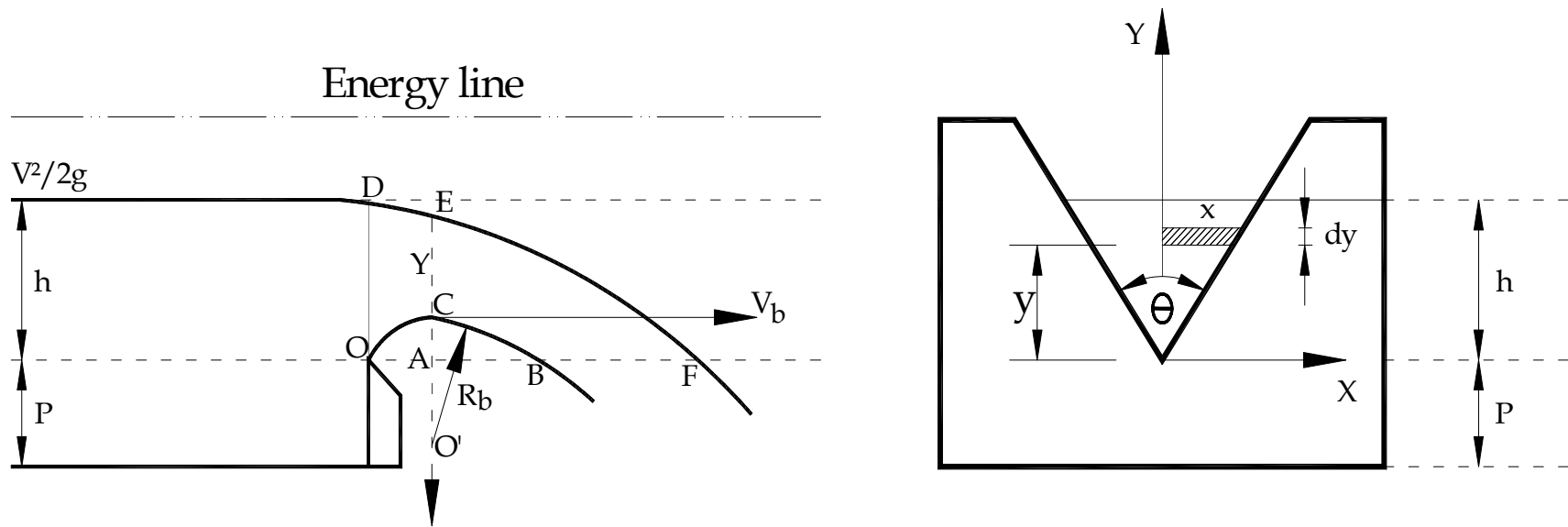




**Figure 2.** Upper and lower nappe profiles. Weir vertex angles: a) 30°, b) 45°, c) 60°, and d) 90°.

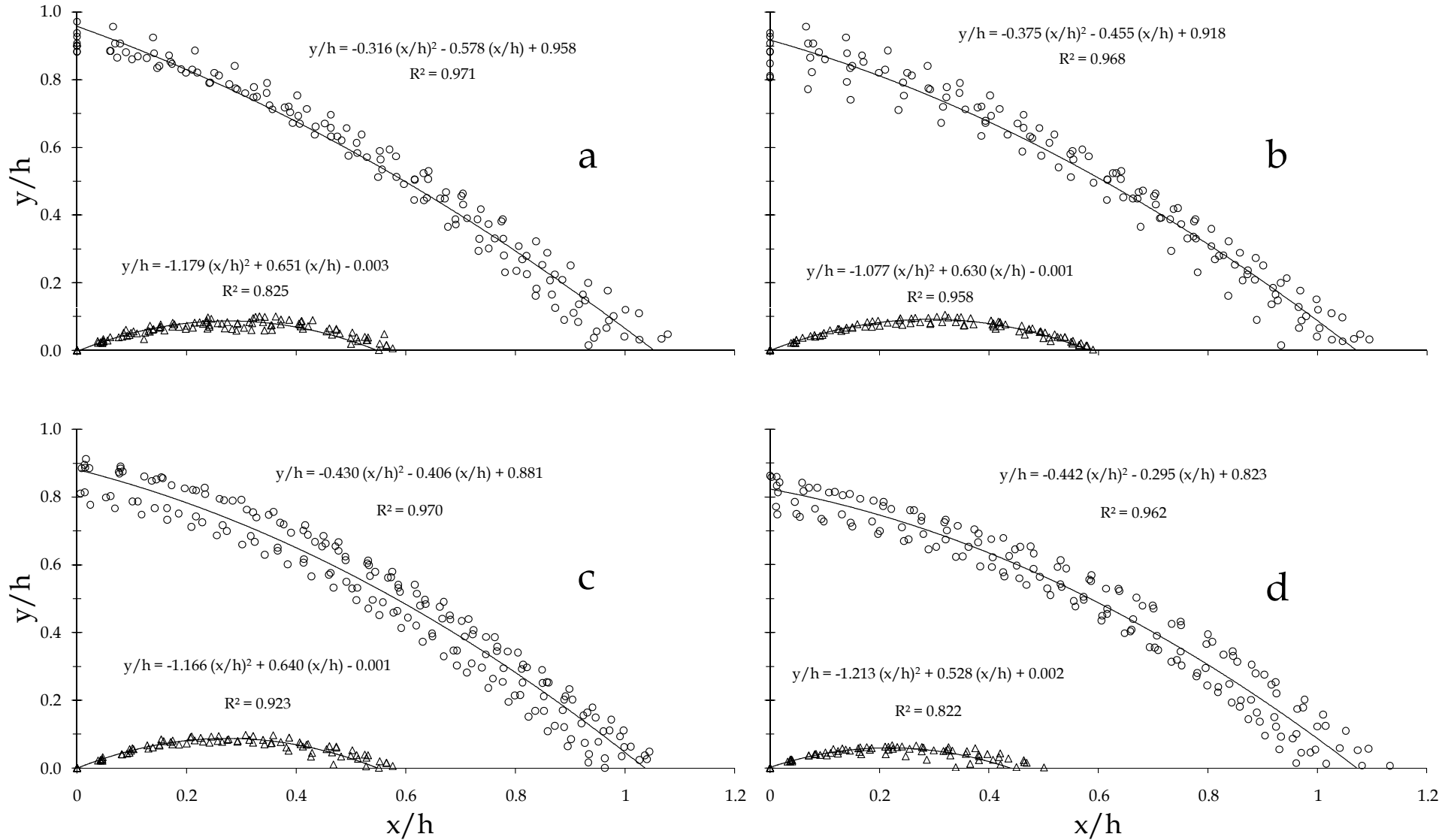


**Figure 3.** Discharge coefficient ( $C_d$ ) vs. head over triangular sharp-crested weir. Weir vertex angles: a)  $30^\circ$ , b)  $45^\circ$ , c)  $60^\circ$ , and d)  $90^\circ$ .

